GEOPHYSICS, VOL. 83, NO. 5 (SEPTEMBER-OCTOBER 2018); P. MR309–MR316, 7 FIGS., 3 TABLES.
10.1190/GEO2018-0071.1

Numerical analysis of local strain measurements in fluid-saturated rock samples submitted to forced oscillations

Samuel Chapman[1] and Beatriz Quintal[1]

ABSTRACT

The forced oscillation method is used to experimentally study the viscoelastic behavior of fluid-saturated rocks at seismic frequencies by measuring their dynamic stress-strain response. The strain on a sample can be measured locally with strain gauges or on the entire sample, here referred to as bulk strain, with a displacement transducer. The local response can vary greatly from the bulk because of heterogeneities in the rock, which can be structural in nature, for example, fractures, or they can arise from partial fluid saturation. Comparing the results from experimental setups that measure strains by different methods can therefore become problematic, and setups that exclusively measure local strains can be inadequate for performing certain experiments. To better understand these limitations, we numerically simulate forced oscillation tests on models representative of laboratory samples, using Biot's quasistatic equations for poroelastic media. The main objective is to analyze the discrepancies that can arise between local and bulk measurements, with a specific focus on the frequency-dependent attenuation and the Young's modulus dispersion. We find that, for a fully water-saturated sample having a single fracture and for a partially saturated sample, the local responses deviate significantly from the bulk responses. In addition, the average of three local measurements along a sample allows for approximating the bulk response for the case of a partially water-saturated sample having a homogeneous solid frame. Such an average is not sufficient for the fractured sample. In summary, the averaging of local strain measurements can provide a partial solution to accurately characterize the dynamic stress-strain response of the sample in certain cases, but in other cases, it can lead to results that strongly deviate from the bulk measurements. We advocate for experimental setups to be built to measure the bulk strain on rock samples or modified to include this measurement in addition to local ones.

INTRODUCTION

Studying mechanical wave attenuation (Q^{-1}) at seismic frequencies in the laboratory is challenging, primarily because the typical seismic wavelength far exceeds the rock sample size. By measuring instead the stress-strain response under sinusoidal loading, one can get around the discrepancy between the seismic wavelength and the sample size. The forced oscillation method (e.g., McKavanagh and Stacey, 1974) infers the attenuation from the phase shift between the stress and strain signals, whereas the stiffness moduli are inferred from the stress and strain amplitudes. Commonly, a uniaxial deformation is applied to the sample; however, volumetric (e.g., Adelinet et al., 2010) and shear (e.g., Behura et al., 2007; Saltiel et al., 2017) deformations can also be performed. With a focus on uniaxial deformations, how the stress and strain on a sample are measured can vary from one experimental setup to another (e.g., Subramaniyan et al., 2014), potentially limiting the types of samples and experimental conditions that can be adequately investigated. In particular, the strain can be measured either locally on a sample with strain gauges (e.g., Batzle et al., 2006; Adelinet et al., 2010; Mikhaltsevitch et al., 2016; Szewzyck et al., 2016) or the bulk deformation of the sample can be measured with some form of displacement transducer (e.g., Spencer, 1981; Paffenholz and Burkhardt, 1989; Tisato and Madonna, 2012; Madonna and Tisato, 2013; Nakagawa, 2013). Strain gauges have the advantage of being less sensitive to resonances in the experimental setup than other transducers (Batzle et al., 2006), and they can directly measure the radial and axial surface strains on a sample. For isotropic and homogeneous samples, this also allows for inferring the bulk and shear moduli from the Young's modulus and Poisson's ratio. In contrast, bulk measurements are largely restricted to axial deformations.

Manuscript received by the Editor 30 January 2018; revised manuscript received 25 April 2018; published ahead of production 28 June 2018; published online 03 September 2018.
[1]University of Lausanne, Institute of Earth Sciences, Lausanne, Switzerland. E-mail: samuel.chapman@unil.ch; beatriz.quintal@unil.ch.

Fluid-saturated rocks behave viscoelastically in the seismic frequency range (e.g., Chapman et al., 2016), resulting in frequency-dependent attenuation and stiffness modulus dispersion. One motivation for conducting forced oscillation experiments is to better understand the physical mechanisms causing the viscoelastic response. A likely mechanism is fluid pressure diffusion associated with the equilibration of fluid pressure gradients induced between regions of different compressibility in the rock (Müller et al., 2010). These contrasts in compressibility can arise from structural heterogeneities in the solid frame as well as when multiple fluids are present in the pore space of the rock. The length scale of such heterogeneities can vary from the pore scale, in the form of microscopic cracks and grain contacts (O'Connell and Budiansky, 1977; Murphy et al., 1986), to the mesoscopic scale, such as fractures and fluid patches (White, 1975; Brajanovski et al., 2005). Because strain gauges cover only a small portion of the surface of a sample, their use is largely limited to investigating pore-scale processes. By taking the average of multiple local strain measurements at different positions on the surface of a sample, the bulk mechanical properties of a rock could possibly be approximated (Adam and Batzle, 2008). Such an approach, however, does not appear to have been thoroughly evaluated or discussed.

The effect of mesoscopic heterogeneities on attenuation and modulus dispersion can be studied by numerically solving Biot's quasistatic equations (Biot, 1941) for models representing a rock sample (e.g., Tisato and Quintal, 2013; Quintal et al., 2017). By using these quasistatic equations, we ignore dynamic effects such as attenuation and modulus dispersion caused by Biot's global flow (Biot, 1962) and scattering (Quintal et al., 2011). These effects are largely negligible at seismic frequencies for the rock and fluid properties, which we will consider in this study (e.g., Berryman, 1985; Bourbié et al., 1987). Tisato and Quintal (2013) and Quintal et al. (2017) use the mentioned numerical methodology to interpret laboratory measurements of seismic attenuation based on bulk strain measurements for partially water-saturated Berea sandstone samples. They explain the laboratory observations to be consistent with mesoscopic-scale heterogeneities in water saturation.

We wish to present a brief analysis of the effect of measuring local strains by numerically simulating forced oscillation tests on models that are representative of laboratory samples. We investigate how the results for frequency-dependent attenuation and modulus dispersion, obtained with local strain measurements, deviate from those obtained with bulk measurements, considering scenarios in which fluid pressure diffusion occurs at the mesoscopic scale. We access three scenarios: (1) a fully water-saturated rock sample with drained top and bottom boundaries, in which attenuation is associated with the drained-to-undrained transition, (2) an undrained rock sample partially saturated with water and air, and (3) an undrained fully water-saturated sample containing a single fracture. We also investigate how well averaging the strains measured at three locations along the sample can approximate the bulk response. Our study is aimed at providing a first quick guide on the effects of local measurements to experimentalists using the forced oscillation method to study frequency-dependent effects in fluid-saturated porous materials.

NUMERICAL METHODOLOGY

Mathematical formulation

We calculate the attenuation and dispersion of the corresponding stiffness modulus caused by fluid pressure diffusion at the mesoscopic scale by numerically solving Biot's (1941) quasistatic equations of poroelasticity in the displacement-pressure (u-p) formulation (Quintal et al., 2011). These equations in the frequency domain are

$$\nabla \cdot \boldsymbol{\sigma} = 0, \tag{1}$$

$$\nabla \cdot \left(-\frac{k}{\eta}\nabla p\right) + \alpha\nabla.(I\omega\mathbf{u}) + \frac{I\omega p}{M} = 0, \tag{2}$$

where I is the imaginary unit; ω is the angular frequency; the symbol p represents the fluid pressure; $\mathbf{u}$ is the vector of solid displacement with its components u_i in the ith directions (e.g., for the 3D case, $i = x, y, z$); and $\boldsymbol{\sigma}$ is the total stress tensor with components (Biot, 1962):

$$\sigma_{ij} = 2\mu\varepsilon_{ij} + \lambda e\delta_{ij} - \alpha p\delta_{ij}, \tag{3}$$

where δ_{ij} is the Kronecker delta, ε_{ij} are the components of the strain tensor, and e is the cubical dilatation given by the trace of the strain tensor. The material properties are the permeability k, the fluid viscosity η, the Lamé's parameters μ and λ, with μ representing the shear modulus of the dry frame and $\lambda = K–2\mu/3$, where K represents the bulk modulus of the dry frame. The Biot-Willis coefficient α and the coefficient M or the reciprocal of the constrained specific storage coefficient (Biot and Willis, 1957) are given by

$$\alpha = 1 - \frac{K}{K_s}, \tag{4}$$

$$M = \left(\frac{\phi}{K_f} + \frac{\alpha - \phi}{K_s}\right)^{-1}, \tag{5}$$

where K_s represents the bulk modulus of the solid grains, K_f represents the bulk modulus of the fluid, and ϕ denotes the porosity.

Numerical solution and deformation mode

We solve equations 1 and 2 in the frequency domain using the finite-element method, by inputting the weak formulation of these equations (Quintal et al., 2011) into the Mathematics module of COMSOL Multiphysics. The weak formulation incorporates Neumann boundary conditions, naturally setting the fluid flow to zero at the boundaries, in other words, allowing our numerical models to have undrained boundaries, unless explicitly stated otherwise. Furthermore, we consider 2D or 3D numerical models, for which we use unstructured meshes with triangular or tetrahedral elements, respectively.

We apply boundary conditions for the solid displacement to our numerical models to represent, for example, uniaxial compression or shear tests to compute the associated complex stiffness moduli. The P-wave modulus can be computed by imposing a zero horizontal displacement to the lateral boundaries of a 2D rectangular model or to the curved lateral boundary of a 3D cylindrical model. In addition, a homogeneous time-harmonic oscillatory displacement (e.g., Milani et al., 2016) is applied on the top boundary of a model, whereas a zero vertical displacement is imposed on the bottom boundary. Finally, the complex P-wave modulus at each frequency is calculated as the ratio between the spatially averaged vertical

stress and the vertical strain obtained from each numerical simulation.

To be consistent with the measurements most often carried out in the laboratory, we focus our analysis on the Young's modulus and the corresponding attenuation. However, to determine the Young's modulus directly requires 3D simulations, whereas the P-wave modulus can be obtained from either 2D or 3D simulations. This is because to compute the Young's modulus, the lateral boundaries of a model must be allowed to move in all horizontal directions, unlike those for the computation of the P-wave modulus, which are fixed with a zero horizontal displacement. Because our 2D problem is equivalent to a 3D case under plane strain conditions, that is, no displacement is allowed to develop in the third dimension, the boundary conditions to directly compute the Young's modulus cannot be satisfied in two dimensions. However, for isotropic models, such as those consisting of a homogeneous solid frame having or not heterogeneities in fluid saturation (Berryman and Wang, 2001), the Young's modulus (E) can be obtained from the P-wave (H) and shear (μ) moduli according to the following relation:

$$E = \frac{\mu(3H - 4\mu)}{H - \mu}. \tag{6}$$

Under these conditions, the shear modulus is equal to that of the drained material according to Gassmann's (1951) equations (Berryman, 1999). For such isotropic models, we perform numerical simulations on 2D models to obtain the P-wave modulus and then we calculate the Young's modulus using equation 6 and Gassmann's prediction for the shear modulus. For anisotropic models, we cannot use such simple relationships between the moduli. Therefore, we perform numerical simulations on 3D models with the appropriate boundary conditions to directly obtain the Young's modulus. The attenuation associated with any stiffness moduli is obtained from the ratio between its imaginary and real parts (O'Connell and Budiansky, 1978).

RESULTS AND DISCUSSION

Drained-to-undrained transition

We first validate our numerical approach with respect to the drained-to-undrained transition (Pimienta et al., 2016). A uniaxial compression test is simulated on a 2D numerical model representing a Berea sandstone sample fully saturated with water and having a homogeneous solid frame (Tables 1 and 2). The model has a length of 25 cm and a diameter of 7.6 cm. By setting the fluid pressure to zero at the top and bottom boundaries, we allow fluid to flow across them, constituting open or drained boundaries. In the numerical simulation, we average the vertical components of the stress and strain fields either over the complete sample length, constituting the bulk response, or over a slice of 1 cm thickness, representative of the local response. In the analytical solution (AS), the local response is calculated at a single point.

In Figure 1, we show results of the AS and numerical solution (NS) for the bulk response (Figure 1a) and the local responses (Figure 1b) at 50% and 75% of the sample length for the Young's modulus (E) and the corresponding attenuation. Due to the symmetry of our model, we do not show the response at 25% of the sample length, which is identical to that at 75%. We observe a satisfactory agreement between the numerical and analytical results, for the bulk and the local measurements. In Figure 1b, we can already observe that a local measurement of strain can lead to inferring attenuation and Young's modulus that deviates from the bulk response of the

Table 1. Physical properties of the solid frame.

Symbol	Property	Berea sandstone	Fracture
K_s	Bulk modulus of the solid grains (GPa)	36	36
ϕ	Porosity (%)	18	50
k	Permeability (mD)	50 (5*)	10,000
K	Bulk modulus of the dry frame (GPa)	7.9	0.025
μ	Shear modulus of the dry frame (GPa)	7.7	0.02

*Background permeability for the fractured sample.

Table 2. Physical properties of the fluids.

Symbol	Property	Water	Air
η	Viscosity of the fluid (Pa × s)	0.001	2×10^{-5}
K_f	Bulk modulus of the fluid (GPa)	2.2	10^{-4}

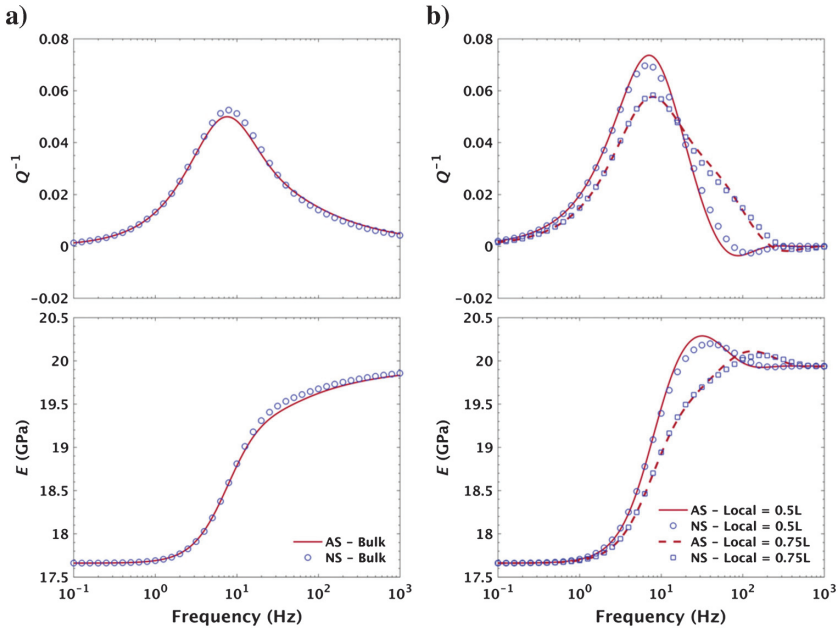

Figure 1. Attenuation and the real part of the Young's modulus obtained with the AS of the drained-to-undrained transition (Pimienta et al., 2016) and with the NS for a fully water-saturated model with open or drained top and bottom boundaries. AS and NS for (a) the bulk response and (b) the local response at 50% and 75% of the sample length (L).

sample even when matrix and fluid heterogeneities are absent but boundaries are open. The attenuation peak of the local response at 50% of the sample length is elevated with respect to that of the bulk response. In addition, the scaling of attenuation with frequency is sensitive to the location of the measurement, especially the high-frequency asymptote. In this case, the local and bulk responses from the Young's modulus converge to the same high- and low-frequency limits. The discrepancies between the local and bulk responses can be understood in terms of the local response failing to fully capture the fluid pressure diffusion occurring from the center to the top and bottom boundaries of the sample.

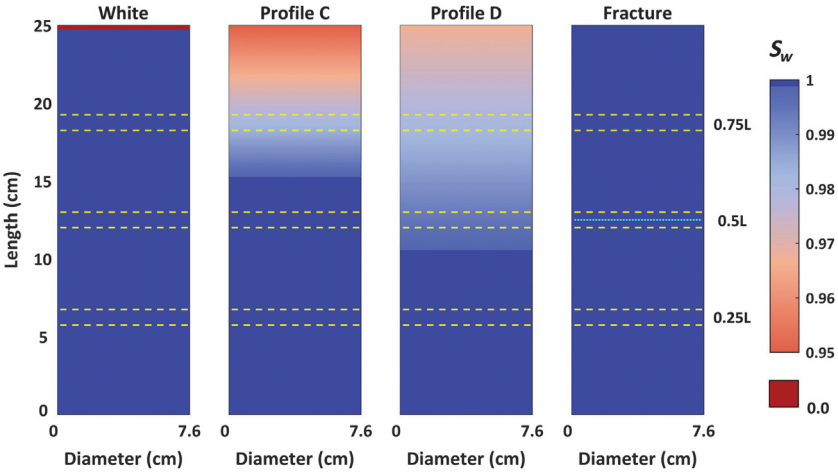

Figure 2. Water-saturation distributions in the numerical models. The overall water saturation for the White, profile C, and profile D is 99%. In the White profile, 99% of the model length is fully water saturated, whereas the top 1% of the model length is fully air saturated. Profiles C and D each have a layer fully saturated with water and a layer in which the water saturation linearly decreases toward the top of the model, described by an effective single-phase fluid (Quintal et al., 2017). The last model is fully water saturated, and a horizontal fracture (the dotted cyan line) of 1 mm thickness is placed at its center. The dashed yellow lines indicate the regions of 1 cm thickness over which the stress and strain responses are averaged to represent a local measurement similar to a strain gauge, located at 25%, 50%, and 75% of the sample length (L).

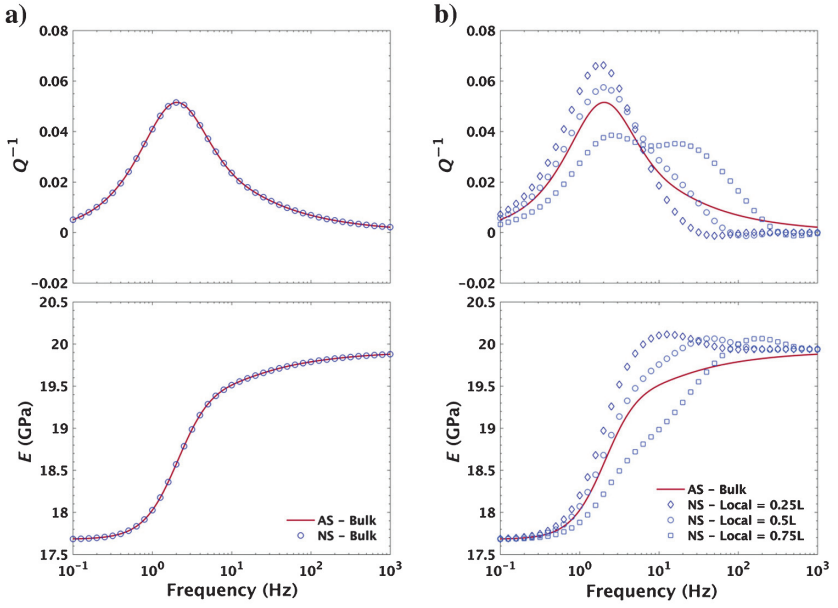

Figure 3. Attenuation and the real part of the Young's modulus obtained from the AS of the interlayer flow model (White et al., 1975) and the NS. The water saturation is 99% with a distribution corresponding to the White profile in Figure 2, and all boundaries are closed or undrained. AS and NS for (a) the bulk response and for (b) the local response at 25%, 50%, and 75% of the sample length (L).

Partial saturation

We now also validate the numerical approach with respect to the case of a partially saturated and sealed Berea sandstone sample. In the 2D numerical model, we represent partial saturation with two horizontal layers, in which a thick lower layer is fully saturated with water and a thin upper layer is fully saturated with air (Tables 1 and 2). Such a fluid distribution corresponds to that of the interlayer flow model (White et al., 1975), and it is shown in Figure 2. In our specific configuration, the overall water saturation of the sample is 99%, where the fully water-saturated layer constitutes 99% and the fully air-saturated layer constitutes 1% of the sample length. All boundaries of the sample are closed or undrained.

The good agreement for attenuation and Young's modulus dispersion between the numerical result based on bulk measurements and the AS (Quintal et al., 2009) for the interlayer flow model validates the numerical approach for the case of partial saturation (Figure 3a). In Figure 3b, we show the local response of the attenuation and Young's modulus, determined at 25%, 50%, and 75% of the sample length. At 25% and 50% of the sample length, the local attenuation is slightly elevated relative to the bulk response, whereas at 75% of the sample length, the locally derived attenuation is lower and appears to display two peaks. In the Young's modulus, the local responses also show more variable frequency dependence than the bulk response, corresponding with the behavior of the attenuation curves, but they converge to the low- and high-frequency limits of the bulk measurement, as observed already for the case shown in Figure 1. The convergence of the limits is associated with the location of the strain measurements in the regions fully saturated by water.

Of course, the binary fluid distribution given by the interlayer flow model does not well reflect a fluid distribution achieved in the laboratory by imbibition. As an approximation, it is reasonable to assume that during imbibition of water into the base of a sample, the water saturation would be greatest at the bottom of the sample and gradually decrease toward the top of the sample. Profiles C and D in Figure 2 describe such a type of distribution while the overall water saturation of the sample remains at 99%, with the rock and fluid properties given in Tables 1 and 2. An effective single-phase fluid describes the gradual

change in water saturation, in which the bulk modulus of such a fluid is based on Wood's (1955) law:

$$K_f = \left(\frac{S_a}{K_a} + \frac{S_w}{K_w}\right)^{-1}, \tag{7}$$

where the subscripts f, a, and w correspond to the effective single-phase fluid, air, and water, respectively. The symbols S and K refer to the saturation and bulk modulus of the respective fluids, respectively. Because only air and water saturate the rock model, $S_a + S_w = 1$. The viscosity of our effective fluid is described by Teja and Rice (1981) as

$$\eta_f = \eta_a \left(\frac{\eta_w}{\eta_a}\right)^{S_w}. \tag{8}$$

The two water distributions given by profiles C and D were previously used by Quintal et al. (2017) to interpret the laboratory measurements by Chapman et al. (2016) and assess the potential impact of open lateral boundaries on the data. Chapman et al. (2016) use the forced oscillation method to measure the dynamic stress-strain response of a partially water-saturated Berea sandstone. The cylindrical sample had a length of 25 cm and a diameter of 7.6 cm. In their experimental setup, a calibrated strain gauge cantilever measured the bulk axial strain on the sample.

In Figure 4, we show the attenuation and Young's modulus measured in the partially saturated Berea sandstone, submitted to 2 MPa confining pressure, by Chapman et al. (2016) and the results of the numerical simulations considering profiles C and D (Figure 2) with closed or undrained boundaries. The numerically derived Young's modulus was offset from the one measured in the laboratory because the bulk and shear moduli of the dry frame (Table 1) do not correspond precisely to those of the used sample; however, the amplitudes of the dispersion were consistent. We therefore normalize the Young's modulus in Figure 4. The numerical and laboratory results for attenuation are also in reasonable agreement with respect to the frequency dependence and amplitude.

We now consider the local responses of attenuation and Young's modulus for profiles C and D at 25%, 50%, and 75% of the sample length (Figure 5). The bulk response, already shown in Figure 4, is shown again in Figure 5 for comparison. At 25% of the sample length, for both profiles, the attenuation is significantly overestimated with respect to the bulk response, and the Young's modulus is correspondingly more dispersive. At 50% of the sample length in profile C, the attenuation curve displays two peaks. The Young's modulus is again more dispersive than the bulk response. In profile D, the local attenuation at 50% of the sample length is overall negligible but it even shows some low negative values, and the Young's modulus is nondispersive. For both profiles at 75% of the sample length, the attenuation is negligible, and the Young's modulus is nondispersive. In summary, attenuation and Young's modulus determined based on local strain measurements can deviate very strongly from results based on bulk measurements. Furthermore, for the same overall water saturation of 99%, but with a minor difference in how the fluids are distributed, not only the locally determined attenuation and Young's modulus can be very different but also the ones based on bulk measurements.

The results presented in Figure 5 indicate that locally measuring the strain on a partially saturated sample can result in inferring frequency-dependent attenuation, and Young's moduli that differ substantially from the bulk response. Measuring the bulk strain on a sample is challenging, and more commonly the local strain is measured by using strain gauges (e.g., Batzle et al., 2006; Adelinet et al., 2010; Mikhaltsevitch et al., 2016; Szewzyck et al., 2016). Adam and Batzle (2008) propose using multiple strain gauges at different locations and taking an average of their responses to approximate the bulk response. We test whether such an average would yield attenuation and Young's modulus results that resembled those obtained with a bulk measurement for profiles C (Figure 6a) and D (Figure 6b). As references for comparison, we again show the bulk response and the local response at 50% of the sample length. For both profiles, averaging the response of the three local measurements at 25%, 50%, and 75% of the sample length significantly improves the inferred attenuation and Young's modulus with respect to the bulk response. The result for Young's modulus, in particular, is close to the sensitivity that one can achieve in the laboratory (e.g., Borgomano et al., 2017). The resulting attenuation for profile C (Figure 6a) is comparable with the bulk response in

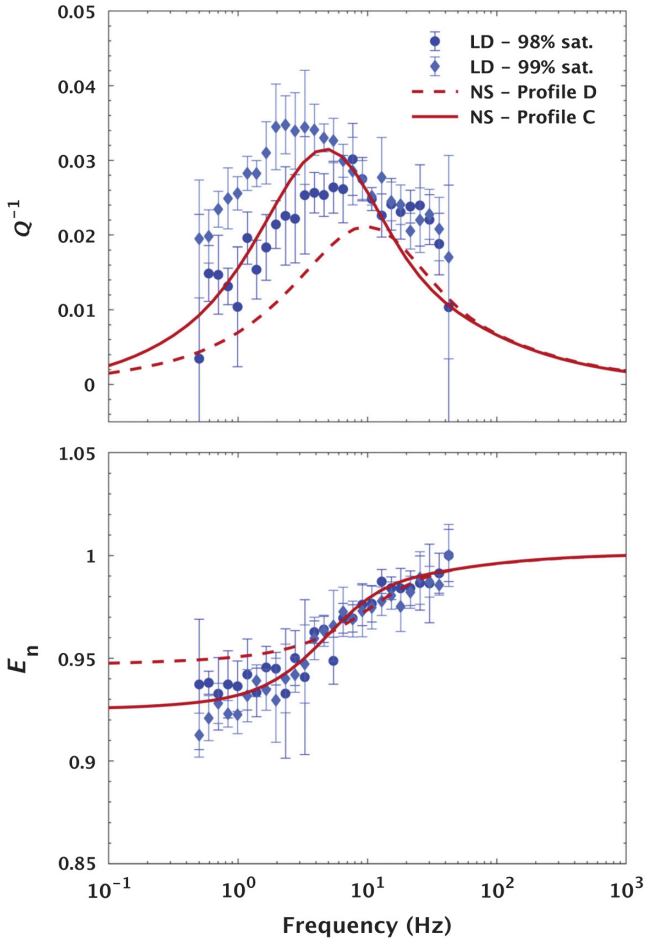

Figure 4. Attenuation and real part of Young's modulus obtained from the NS considering the bulk response for water saturation profiles C and D (Figure 2) corresponding to 99% total water saturation. The laboratory data (LD) are from Chapman et al. (2016) for a Berea sandstone sample with approximate water saturations of approximately 98% and 99%, subjected to 2 MPa confining pressure. The Young's modulus has been normalized with respect to its highest value.

amplitude and matches well the transition frequency. In contrast, the attenuation for profile D (Figure 6b) is improved but underestimated with respect to the bulk response. Overall, by taking an average of the local responses measured at the three locations, the inferred attenuation and Young's modulus are improved compared with that based on local measurements at any of the three locations.

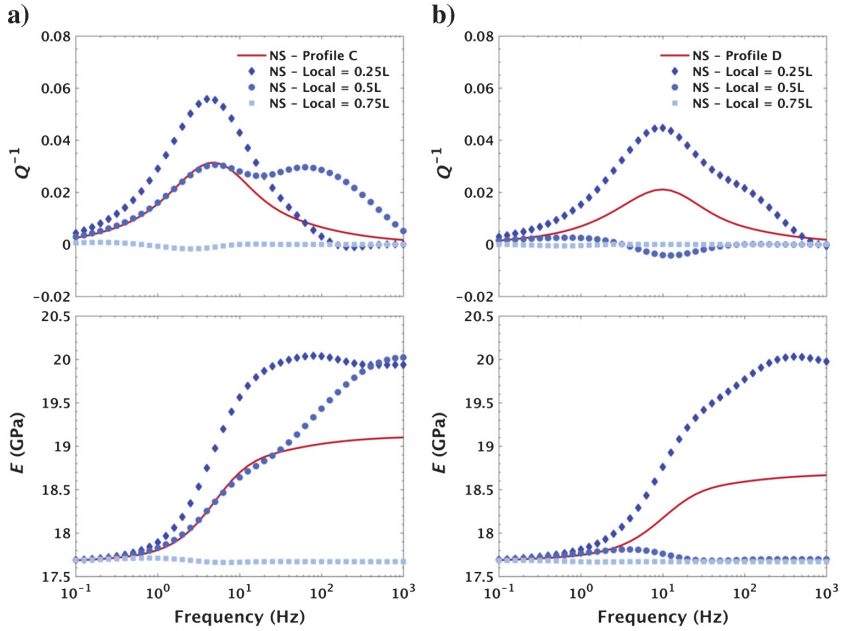

Figure 5. Attenuation and real part of Young's modulus obtained from the NS for water saturation profiles (a) C and (b) D (Figure 2), corresponding to 99% total water saturation, considering the bulk and local responses at 25%, 50%, and 75% of the sample length (L).

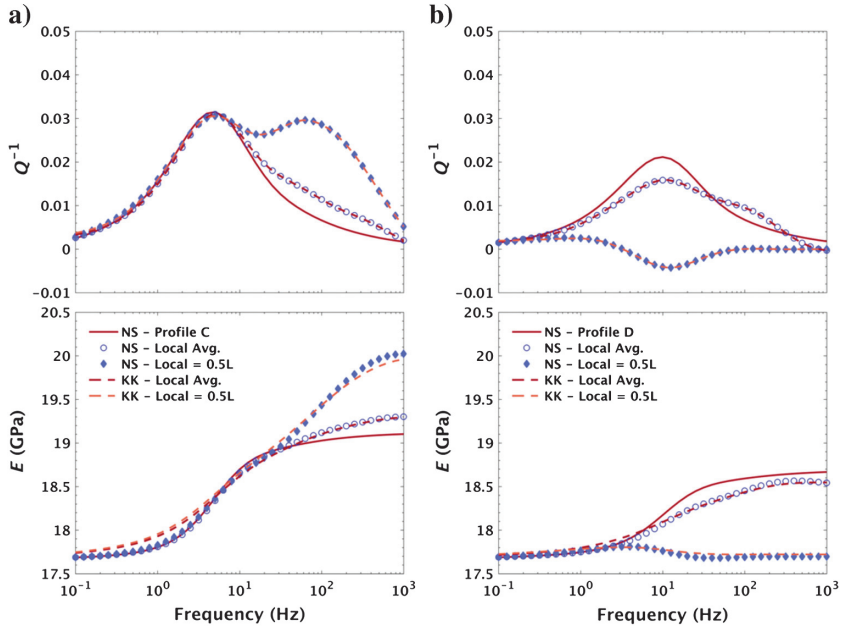

Figure 6. Attenuation and real part of Young's modulus obtained from the NS for the water saturation profiles (a) C and (b) D (Figure 2) corresponding to 99% total water saturation. We consider the bulk response and local response at 50% of the sample length (L), and the average of the local responses at 25%, 50%, and 75% of the sample length (L). Results obtained based on the KK relations (Mikhaltsevitch et al., 2016) applied to the NS of the local and averaged responses are also shown.

In Figure 6, we also show that the results based on local measurements follow the Kramers-Kronig (KK) relations (Mikhaltsevitch et al., 2016), even for results that would seem physically improbable such as the negative attenuation values obtained at 50% of the sample length considering profile D. The agreement with the KK relations reflects that the local signature of fluid pressure diffusion in such a heterogeneous sample is correct, but it merely and obviously cannot reflect the physical phenomenon taking place in the whole sample. In fact, attenuation and dispersion measurements using the forced oscillations method are based on the assumption that the probed material behaves viscoelastically at an observation (or measurement) scale, which is larger than that where the dissipative fluid pressure diffusion occurs (Jänicke et al., 2015).

Fractured media

Heterogeneities in a sample can also arise in the solid frame of the rock and not only from the distribution of different fluids. To investigate the impact of a fracture on the local and bulk responses of attenuation and Young's modulus, we performed numerical simulations on a 3D cylindrical model considering full water saturation (Table 2). All boundaries of the model are again closed or undrained. The fracture is approximated as a very thin layer having a much more compliant, more porous, and more permeable solid frame than the embedding background that has properties of Berea sandstone with a relatively low permeability of 5 mD (Table 1). The fracture is placed at the center of the model with a thickness of 1 mm, and it is orientated perpendicular to the vertical axis (Figure 2).

We once again validate our numerical results by comparing the bulk numerical response to the AS of the interlayer flow model (White et al., 1975; Quintal et al., 2009). With the presence of a fracture, the model no longer behaves isotropically, and thus we cannot calculate the Young's modulus from the P-wave and shear moduli using relationships for isotropic elastic materials, as done before. Therefore, we first compare the numerically and analytically derived P-wave modulus and corresponding attenuation (Figure 7a), successfully validating our 3D numerical scheme. The amplitude of P-wave attenuation in a medium fully saturated with a liquid and containing fractures, which are perpendicular to the direction of deformation, is mainly controlled by the contrast in compressibility between the solid frame of the background and that of the fracture (Müller et al., 2010; Ru-

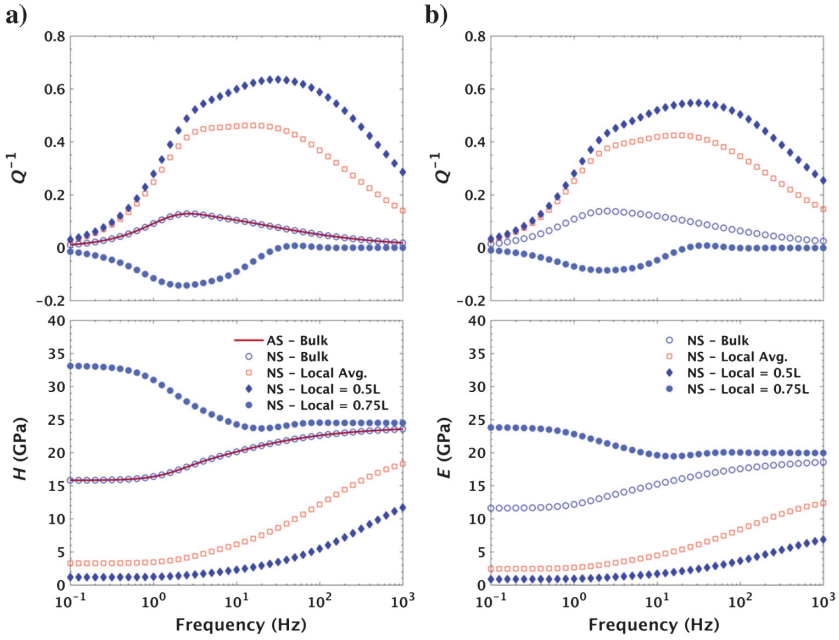

Figure 7. (a) Attenuation and corresponding real part of the P-wave modulus and (b) attenuation and the corresponding real part of the Young's modulus for the fully water-saturated cylindrical model having a single horizontal fracture at its center. The NS and AS solutions of the interlayer flow model (White et al., 1975) are given for the P-wave modulus. The numerically calculated local responses at 50% and 75% of the model length as well as the average of the local responses at 25%, 50%, and 75% of the sample length (L) are also shown.

bino et al., 2014). The characteristic frequency of the attenuation peak is controlled by the permeability and length of the embedding background and by the viscosity of the saturating liquid (Brajanovski et al., 2006).

In Figure 7a, we also show the local responses at 50% and 75% of the sample length for the P-wave modulus and the corresponding attenuation. Because of the symmetry of our model, we do not show the response at 25% of the sample length, which is identical to that at 75%. The average response comprises the three local measurements as previously done for the partially saturated models (Figure 6). As expected, the local responses deviate substantially from the bulk response for the attenuation and P-wave modulus. Unlike for partial saturation (Figure 6), the average of the local responses also significantly deviates from the bulk response.

The Young's modulus and the corresponding attenuation are computed as well by changing the boundary conditions applied to the curved lateral surface of cylindrical model, allowing for unconstrained horizontal displacements. We observe that the local responses and their average also differ substantially from the bulk response (Figure 7b), similarly as observed for the P-wave modulus case (Figure 7a).

CONCLUSION

The numerical results show that the local and bulk measurements of attenuation and Young's modulus differ substantially for partially saturated and fractured samples. Such a response is expected because the dissipative fluid pressure diffusion in these models takes place across portions of the samples that are much larger than the portion probed in the case of local measurements. Experimental setups using the forced oscillation method are therefore limited with respect to the types of samples and fluid distributions that they can investigate if the strains are measured locally. Furthermore, given the small number of such experimental setups available, it becomes difficult to independently verify some experiments.

As a possible solution for setups capable of only measuring local strains, we investigated whether the bulk response could be approximated by averaging the local responses from three locations along a sample. For the partially saturated samples, using a simplified fluid distribution, the bulk response could be approximated by such an average. For the fractured sample, which was fully water saturated, taking the average of three local measurements was not sufficient to obtain a reasonable approximation of the bulk results.

It should be noted that the dimensions of the samples considered here are those of the largest samples that can be measured with the currently available experimental setups based on the forced oscillation method. The differences between the local and bulk responses are obviously more pronounced for larger samples if we consider a single size of strain gauges. For smaller samples, the averaging approach should lead to better results because larger fractions of the samples are probed by the local measurements. However, measuring the bulk response is in any case undoubtedly preferred.

From a different perspective, the strong deviations that local measurements exhibit compared with bulk measurements could be helpful in assisting in the interpretation of laboratory measurements. For example, a combination of measuring local and bulk strains on a sample could perhaps be used to distinguish between microscopic and mesoscopic sources of attenuation and modulus dispersion.

ACKNOWLEDGMENTS

This work was supported by a grant from the Swiss National Science Foundation. We thank L. Pimienta for the many discussions and for providing the impetus for this work. We also wish to thank H. Yin and two other anonymous reviewers.

DATA AND MATERIALS AVAILABILITY

Data associated with this research are available and can be obtained by contacting the authors.

REFERENCES

Adam, L., and M. Batzle, 2008, Elastic properties of carbonates from laboratory measurements at seismic and ultrasonic frequencies: The Leading Edge, **27**, 1026–1032, doi: 10.1190/1.2967556.

Adelinet, M., J. Fortin, Y. Gueguen, A. Schnubel, and L. Geoffroy, 2010, Frequency and fluid effects on elastic properties of basalt: Experimental investigations: Geophysical Research Letters, **37**, L02303, doi: 10.1029/2009GL041660.

Batzle, M. L., D.-H. Han, and R. Hofmann, 2006, Fluid mobility and frequency-dependent seismic velocity — Direct measurements: Geophysics, **71**, no. 1, N1–N9, doi: 10.1190/1.2159053.

Behura, J., M. Batzle, R. Hofmann, and J. Dorgan, 2007, Heavy oils: Their shear story: Geophysics, **72**, no. 5, E175–E183, doi: 10.1190/1.2756600.

Berryman, J. G., 1985, Scattering by a spherical inhomogeneity in a fluid-saturated porous medium: Journal of Mathematical Physics, **26**, 1408–1419, doi: 10.1063/1.526955.

Berryman, J. G., 1999, Origin of Gassmann's equations: Geophysics, **64**, 1627–1629, doi: 10.1190/1.1444667.

Berryman, J. G., and H. F. Wang, 2001, Dispersion in poroelastic systems: Physical Review E, **64**, 011303, doi: 10.1103/PhysRevE.64.011303.

Biot, M. A., 1941, General theory of three-dimensional consolidation: Journal of Applied Physics, **12**, 155–164, doi: 10.1063/1.1712886.

Biot, M. A., 1962, Mechanics of deformation and acoustic propagation in porous media: Journal of Applied Physics, **33**, 1482–1498, doi: 10.1063/1.1728759.

Biot, M. A., and D. G. Willis, 1957, The elastic coefficients of the theory of consolidation: Journal of Applied Mechanics, **24**, 594–601.

Borgomano, J. V. M., L. Pimienta, J. Fortin, and Y. Gueguen, 2017, Dispersion and attenuation measurements of elastic moduli of a dual-porosity limestone: Journal of Geophysical Research: Solid Earth, **122**, 2690–2711, doi: 10.1002/2016JB013816.

Bourbié, T., O. Coussy, and B. Zinszner, 1987, Acoustics of porous media: EditionsTechnip.

Brajanovski, M., B. Gurevich, and M. Schoenberg, 2005, A model for P-wave attenuation and dispersion in a porous medium permeated by aligned fractures: Geophysical Journal International, **163**, 372–384, doi: 10.1111/j.1365-246X.2005.02722.x.

Brajanovski, M., T. M. Müller, and B. Gurevich, 2006, Characteristic frequencies of seismic attenuation due to wave-induced fluid flow in fractured porous media: Geophysical Journal International, **166**, 574–578, doi: 10.1111/j.1365-246X.2006.03068.x.

Chapman, S., N. Tisato, B. Quintal, and K. Holliger, 2016, Seismic attenuation in partially saturated berea sandstone submitted to a range of confining pressures: Journal of Geophysical Research: Solid Earth, **121**, 1664–1676, doi: 10.1002/2015JB012575.

Gassmann, F., 1951, Über die Elastizität poröser Medien: Vierteljahrsschrift der Naturforschenden Gesellschaft in Zürich, **96**, 1–23.

Jänicke, R., B. Quintal, and H. Steeb, 2015, Numerical homogenization of mesoscopic loss in poroelastic media: European Journal of Mechanics A/Solids, **49**, 382–395, doi: 10.1016/j.euromechsol.2014.08.011.

Madonna, C., and N. Tisato, 2013, A new seismic wave attenuation module to experimentally measure low-frequency attenuation in extensional mode: Geophysical Prospecting, **61**, 302–314, doi: 10.1111/1365-2478.12015.

McKavanagh, B., and F. D. Stacey, 1974, Mechanical hysteresis in rocks at low strain amplitudes and seismic frequencies: Physics of the Earth and Planetary Interiors, **8**, 246–250, doi: 10.1016/0031-9201(74)90091-0.

Mikhaltsevitch, V., M. Lebedev, and B. Gurevich, 2016, Validation of the laboratory measurements at seismic frequencies using the Kramers-Kronig relationship: Geophysical Research Letters, **43**, 4986–4991, doi: 10.1002/2016GL069269.

Milani, M., J. G. Rubino, T. M. Müller, B. Quintal, E. Caspari, and K. Holliger, 2016, Representative elementary volumes for evaluating effective seismic properties of heterogeneous poroelastic media: Geophysics, **81**, no. 2, D169–D181, doi: 10.1190/GEO2015-0173.1.

Müller, T. M., B. Gurevich, and M. Lebedev, 2010, Seismic wave attenuation and dispersion resulting from wave-induced flow in porous rocks — A review: Geophysics, **75**, no. 5, A147–A164, doi: 10.1190/1.3463417.

Murphy, W. F., III, K. W. Winkler, and R. L. Robert Kleinberg, 1986, Acoustic relaxation in sedimentary rocks: Dependence on grain contacts and fluid saturation: Geophysics, **51**, 757–766, doi: 10.1190/1.1442128.

Nakagawa, S., 2013, Low-frequency (<100Hz) dynamic fracture compliance measurement in the laboratory: 47th US Rock Mechanics/Geomechanics Symposium, ARMA, 13–343.

O'Connell, R. J., and B. Budiansky, 1977, Viscoelastic properties of fluid-saturated cracked solids: Journal of Geophysical Research, **82**, 5719–5735, doi: 10.1029/JB082i036p05719.

O'Connell, R. J., and B. Budiansky, 1978, Measures of dissipation in viscoelastic media: Geophysical Research Letters, **5**, 5–8, doi: 10.1029/GL005i001p00005.

Paffenholz, J., and H. Burkhardt, 1989, Absorption and modulus measurements in the seismic frequency and strain range on partially saturated sedimentary rocks: Journal of Geophysical Research, **94**, 9493–9507, doi: 10.1029/JB094iB07p09493.

Pimienta, L., J. V. M. Borgomano, J. Fortin, and Y. Guéguen, 2016, Modelling the drained/undrained transition: Effect of the measuring method and the boundary conditions: Geophysical Prospecting, **64**, 1098–1111, doi: 10.1111/1365-2478.12390.

Quintal, B., S. Chapman, N. Tisato, and J. Paffenholz, 2017, Numerical analysis of laboratory attenuation measurements: Poromechanics VI: Proceedings of the Sixth Biot Conference on Poromechanics, Paris, France, 1642–1649, doi: 10.1061/9780784480779.203.

Quintal, B., S. M. Schmalholz, and Y. Y. Podladchikov, 2009, Low frequency reflections from a thin layer with high attenuation caused by interlayer flow: Geophysics, **74**, no. 1, N15–N23, doi: 10.1190/1.3026620.

Quintal, B., H. Steeb, M. Frehner, and S. M. Schmalholz, 2011, Quasi-static finite element modeling of seismic attenuation and dispersion due to wave-induced fluid flow in poroelastic media: Journal of Geophysical Research: Solid Earth, **116**, B01201, doi: 10.1029/2010JB007475.

Rubino, J. G., T. M. Müller, M. Milani, and K. Holliger, 2014, Seismic attenuation and velocity dispersion in fractured rocks: The role played by fracture contact areas: Geophysical Prospecting, **62**, 1278–1296, doi: 10.1111/1365-2478.12170.

Saltiel, S., P. A. Selvadurai, B. P. Bonner, S. D. Glaser, and J. B. Ajo-Franklin, 2017, Experimental development of low-frequency shear modulus and attenuation measurements in matted rock fractures: Shear mechanics due to asperity contact area changes with normal stress: Geophysics, **82**, no. 2, M19–M36, doi: 10.1190/geo2016-0199.1.

Spencer, J. W., Jr., 1981, Stress relaxations at low frequencies in fluid saturated rocks: Attenuation and modulus dispersion: Journal of Geophysical Research, **86**, 1803–1812, doi: 10.1029/JB086iB03p01803.

Subramaniyan, S., B. Quintal, N. Tisato, E. H. Saenger, and C. Madonna, 2014, An overview of laboratory apparatuses to measure seismic attenuation in reservoir rocks: Geophysical Prospecting, **62**, 1211–1223, doi: 10.1111/1365-2478.12171.

Szewczyk, D., A. Bauer, and R. M. Holt, 2016, A new laboratory apparatus for the measurement of seismic dispersion under deviatoric stress conditions: Geophysical Prospecting, **64**, 789–798, doi: 10.1111/1365-2478.12425.

Teja, A. S., and P. Rice, 1981, Generalized corresponding states method for viscosities of liquid mixtures: Industrial and Engineering Chemistry Fundamentals, **20**, 77–81, doi: 10.1021/i100001a015.

Tisato, N., and C. Madonna, 2012, Attenuation at low seismic frequencies in partially saturated rocks: Measurements and description of a new apparatus: Journal of Applied Geophysics, **86**, 44–53, doi: 10.1016/j.jappgeo.2012.07.008.

Tisato, N., and B. Quintal, 2013, Measurements of seismic attenuation and transient fluid pressure in partially saturated Berea sandstone: Evidence of fluid flow on the mesoscopic scale: Geophysical Journal International, **195**, 342–351, doi: 10.1093/gji/ggt259.

White, J. E., 1975, Computed seismic speeds and attenuation in rocks with partial gas saturation: Geophysics, **40**, 224–232, doi: 10.1190/1.1440520.

White, J. E., N. G. Mikhaylova, and F. M. Lyakhovitskiy, 1975, Low-frequency seismic waves in fluid-saturated layered rocks: Earth Physics, **10**, 654–659, doi: 10.1121/1.1995164.

Wood, A. W., 1955, A textbook of sound: MacMillan Publishing Company.